Available online at www.sciencedirect.com
ScienceDirect
Journal of Bionic Engineering 11 (2014) 400–411

Gait Study and Pattern Generation of a Starfish-Like Soft Robot with Flexible Rays Actuated by SMAs

Shixin Mao[1], Erbao Dong[1], Hu Jin[1], Min Xu[1], Shiwu Zhang[1], Jie Yang[1], Kin Huat Low[2]

1. *Department of Precision Machinery and Precision Instrumentation*, *University of Science and Technology of China*, *Hefei* 230026, *P. R. China*

2. *School of Mechanical and Aerospace Engineering*, *Nanyang Technological University*, *Singapore* 639798, *Singapore*

Abstract

This paper presents the design and development of a starfish-like soft robot with flexible rays and the implementation of multi-gait locomotion using Shape Memory Alloy (SMA) actuators. The design principle was inspired by the starfish, which possesses a remarkable symmetrical structure and soft internal skeleton. A soft robot body was constructed by using 3D printing technology. A kinematic model of the SMA spring was built and developed for motion control according to displacement and force requirements. The locomotion inspired from starfish was applied to the implementation of the multi-ray robot through the flexible actuation induced multi-gait movements in various environments. By virtue of the proposed ray control patterns in gait transition, the soft robot was able to cross over an obstacle approximately twice of its body height. Results also showed that the speed of the soft robot was 6.5 times faster on sand than on a clammy rough terrain. These experiments demonstrated that the bionic soft robot with flexible rays actuated by SMAs and multi-gait locomotion in proposed patterns can perform successfully and smoothly in various terrains.

Keywords: soft robot, bio-inspiration, multi-gait locomotion, rough terrains, SMA actuators

doi: 10.1016/S1672-6529(14)60053-6

1 Introduction

Robots are traditionally formed by rigid links connected by discrete single-degree-of-freedom rotary or linear actuators. In contrast, soft robots enable scientists to combine a simple design with complex movements. Furthermore, these robots are more resistant to mechanical damage than robots with rigid structure[1–4]. Inspired by various soft-bodied organisms, such as octopus, caterpillar, earthworm, or even the elephant trunk, researchers have developed various bionic robots by employing soft materials and structures. Shepherd *et al.*[5], Correll *et al.*[6], and McMahan *et al.*[7] have developed a soft quadruped robot actuated by a pneumatic drive, a peristaltic robot, and a continuum robot, respectively. Calisti *et al.*[8] have developed an octopus arm robot actuated by motors. Several soft actuators, such as Electro-Active Polymers (EAPs) or gel, Ionic Polymer Metal Composite (IPMC), as well as Shape Memory Alloy (SMA) wires and springs, have also been proposed to improve the compactness and actuation of soft robots[9,10]. EAPs can generate deformations, but require a large electric field and a rigid frame structure. Moreover, they can only produce a small force[9]. IPMC actuators are light and can accomplish large bending displacements. Like EAP, the IPMC actuators can generate only a small force[11]. By contrast, SMA actuators can generate larger displacements with simple mechanisms. In addition, SMA spring actuators exhibit high energy density[12]. Seok *et al.*[11], Shiotsu *et al.*[12], Lin *et al.*[13] respectively developed an earthworm-like robot, a rolling robot, and a caterpillar-inspired robot based on SMA actuators. These robots have compact structures, but they can only move on flat ground due to the limit of their structures and gaits.

Various issues limit the development of soft robots, such as the soft bionic structure, flexible actuation and multi-gait locomotion. Several kinds of soft robots have

Corresponding author: Erbao Dong
E-mail: ebdong@ustc.edu.cn

recently been developed to address the aforementioned issues. However, most of these have done little in enhancing deformability, mobility or adaptability, because they can only grasp objects with a large fixed frame (*e.g.*, octopus and continuum robots[7,8]), move on flat ground (*e.g.*, peristaltic robot[6]), or have a rarely limited gait motion (*e.g.*, inversion motion of a gel robot[10]).

The sea star, which is one of the most familiar marine invertebrates, has a completely symmetrical structure and exhibits multi-gait locomotion, large deformation, and complex environmental adaptability[14–16]. Inspired by these biological observations, we developed a five-ray robot with a soft skeleton and multi-gait locomotion by using SMA actuators. Soft body allows the robot to achieve a high mobility via shape changes, withstand external damages, and adapt to different terrains through passive or active deformation. A kinematic model of SMA actuators was developed, with which an SMA spring could be easily designed and controlled according to force and displacement requirements. The locomotion strategies of the soft robot prototype on different terrain conditions (sand, clammy rough terrain, rough ground, rocks, *etc*.) were studied through extensive experiments. The approach to developing the starfish-like soft robot offers many new features compared to the previously discussed robotic systems.

Two kinds of soft rays were designed and constructed, followed by deformation analysis of the soft ray and modeling of the SMA actuators. Different locomotion strategies and related control strategies were subsequently utilized for the soft robot according to different environmental conditions. Multi-gait experiments were also conducted to verify the capabilities of the robot in various terrains. Finally, the interaction between mobility and environmental terrain was studied by comparing and analyzing the robot prototype under different conditions.

2 Bionic description of starfish

2.1 Mechanism of locomotion

The starfish can be considered as an icon of the sea; however, it also has immense ecological and biological importance[17]. Studies on starfish began in the second half of the 19th century but were limited primarily to evolution, distribution, and growth[17,18]. Cole[19] focused on starfish locomotion. The position of the rays varies during locomotion[19–21]; two rays may be pushed in advance, with three rays following (Fig. 1a), or *vice versa* (Fig. 1b). A sea star may move with any of its rays in the lead or in any intermediate direction; it also exhibits a tendency as it crawls, even over a short course, to change locomotion direction not by turning its body but by changing its front. The variation possibilities in locomotion direction may result in a slightly zigzag movement[22] on coastal beach.

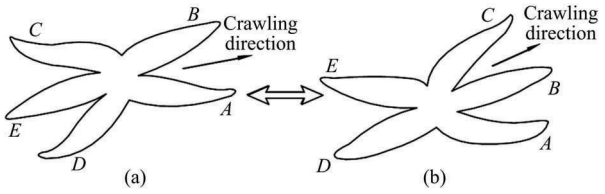

Fig. 1 Diagrams of (a) a sea star crawling with two rays in advance and three rays following, and (b) *vice versa*.

A sea star maintains a delicate internal electrolyte balance that is in equilibrium with seawater, thus allowing it to use different gaits in various environmental conditions, including rocky shores, tidal pools, and mud[18,21,23]. To demonstrate how a sea star can achieve different gaits and move with two rays in advance in various terrains, the serial experiments were conducted, see section **5**.

2.2 Mechanism for crawling

As mentioned earlier, individual starfish exhibit considerable differences in their progression methods. Sometimes, all the rays are arched on the surface, on which a sea star is crawling; other times, the rays are arched upward. A sea star may crawl with two or three rays in advance. To discuss the gait study on the starfish-like soft robot, two flexible rays were pushed in advance during locomotion to explore the principle of multi-gait among soft robots in various terrains. The schematic representation of the principle of basic locomotion is shown in Fig. 2. The corresponding control pattern can be designated by pattern *AB–CD–E*.

For the sake of discussion, the rays were designated by letters *A* to *E*. A period of motion was divided into the following six stages.

Stage 1: Rays *A* and *B* (with gridding) bend and move ahead through the friction between the rays and the ground medium.

Stage 2: Rays *C* and *D* (with gridding) bend; four curving rays simultaneously upraise the body and make the entire body move with ground friction; the center of gravity shifts ahead.

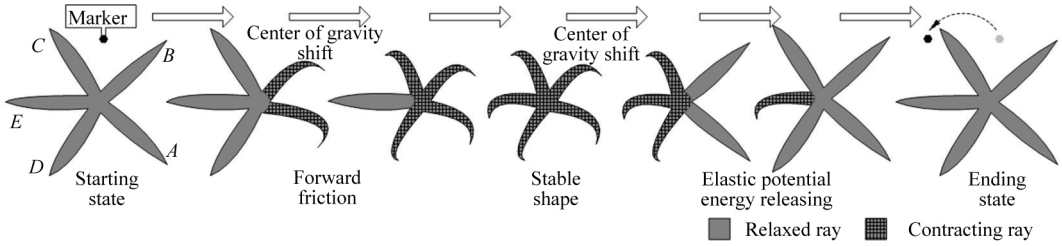

Fig. 2 Mechanism for crawling on sand and creeping on a clammy rough terrain.

Stage 3: Ray *E* (with gridding) bends; the soft body achieves a stable shape and accumulates an elastic potential energy for crawling.

Stage 4: Rays *A* and *B* relax; the center of gravity shifts ahead.

Stage 5: Rays *C* and *D* relax; the released elastic potential energy propels the robot body forward.

Stage 6: Ray *E* relaxes, and the soft robot returns to its initial state; the displacement can be identified by the marker position.

2.3 Mechanism for navigating obstacles

Once a sea star establishes a progression in a definite direction wherein an obstacle is presented, the two rays that are pushed in advance can grasp the obstacle with the help of the other three rays. Fig. 3a describes the entire process for the starfish-like robot — from the initial state to completely negotiating an obstacle. The robot first moves forward by following the pattern *AB–CD–E* before raising its body as soon as it touches the obstacle by following pattern *ABCD–E*, which also helps to produce a walking gait. Finally, the robot continues its trip by following pattern *AB–CD–E*. The corresponding positions of the five rays of the robot are displayed in the figure. The rays (with gridding) depict inactivity (that is, the actuated SMA spring temperature was reduced), whereas the gray rays imply that the rays are active.

A sea star is a typical marine invertebrate with a symmetrical shape that allows it to move in different directions through actuating related rays. Fig. 3b shows the complete process, in which the robot bypasses an impassable rock (its height is more than two times of the starfish's). The process can be divided into four main steps. First, the robot goes forward by following control pattern *AB–CD–E*. Second, the robot turns left and then moves ahead by following control pattern *BC–AE–D*. Third, the robot continues its journey by following control pattern *AD–BE–C* to turn right. Finally, the robot returns to following control pattern *AB–CD–E* and succeeds in bypassing the obstacle.

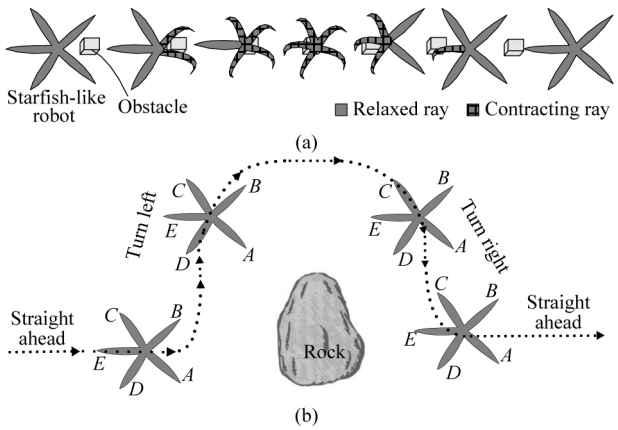

Fig. 3 Gait pattern: (a) Strategy in navigating an obstacle and (b) gait transitions to avoid an impassable obstacle.

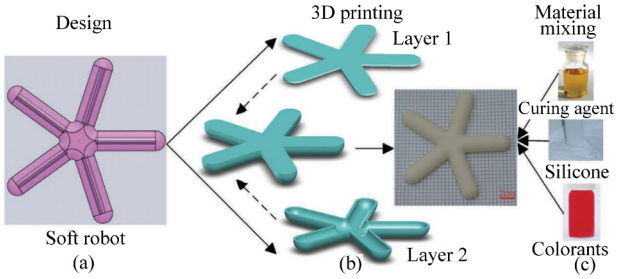

Fig. 4 Schematic representation of the construction process for the soft robot prototype.

3 Bionic structure of soft robot

3.1 Design and construction

A sea star exhibits radial symmetry that radiates outward from the center of its body. Its structure is madreporite, which connects its water-vascular system with its exterior[18,24]. Inspired by the symmetrical structure and the soft internal skeleton of the starfish, the bionic structure of the soft robot with five flexible rays was designed (Fig. 4a). To construct this robot prototype, we adopted a combined model with a sealing layer (layer 1) and a shaping layer (layer 2) constructed via 3D

printing technology by using acrylonitrile butadiene styrene (P430 ABS) plastic molds constructed with a 3D printer (Dimension 1200 SST, Stratasys Inc., Eden Prairie, MN, USA) (Fig. 4b). The lightweight skeleton and tendons of the robot must be strong enough to withstand the forces acting on them during locomotion. Therefore, their elastic properties should be studied.

Fig. 4c illustrates the process for mixing different materials (including curing agent, silicone, and colorants). The mass ratio among curing agent, silicone, and colorants is 3:100:1. The robot prototype was embedded by a special silicone rubber (RTV-2) with moderate suppleness and toughness, which allow the robot to not only support its entire body to achieve different postures, but also to satisfy considerable flexible deformation requirements. The curing agent was used to change the elasticity of the soft body; and the colorants helped to adjust the appearance of the robot according to external conditions.

3.2 Deformation analysis

Fig. 5a presents the robot prototype for deformation analysis. The SMA actuator (with the ultimate tensile strength of 50 MPa and the material is nickel-titanium alloy) was embedded into the flexible ray. The diaphragm seal was applied to prevent the system from leaking water. Fig. 5b illustrates a complete deformation of the soft ray when powered by the SMA actuator. The deformation rate increases gradually at the beginning.

By defining the middle curve length of the bending soft ray as S, the deformation of each ray can be expressed as

$$\mu=S/L, \tag{1}$$

where L is the current length of the SMA spring. Note that the length is inversely proportional to S during the bending of the soft ray.

To obtain the value of μ and the optimal flexible ray structure, two kinds of rays were constructed. The first was sealed by a diaphragm, whereas the second was not sealed. When both rays were powered through the SMA actuator with a current of 1.75 A, the value of μ reached μ_1 (approximately 2.6) within 15 s for the unsealed soft ray (Fig. 6), whereas the value of μ reached μ_2 (approximately 2.0) within 17 s for the sealed soft ray. The former required less than 60 s to restore its initial shape, whereas the latter required 80 s for the same effect.

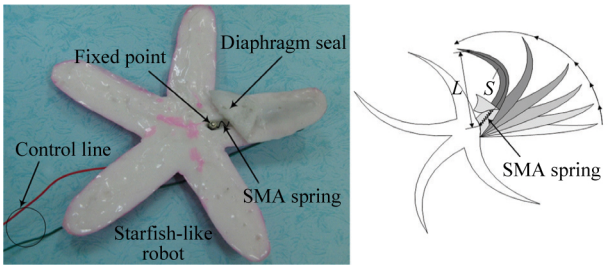

Fig. 5 Bionic structure and deformation analysis. (a) The soft robot with the driving system that mainly consists of the SMA actuators and the soft silicone material ray; (b) diagram of the deformation of a bending ray.

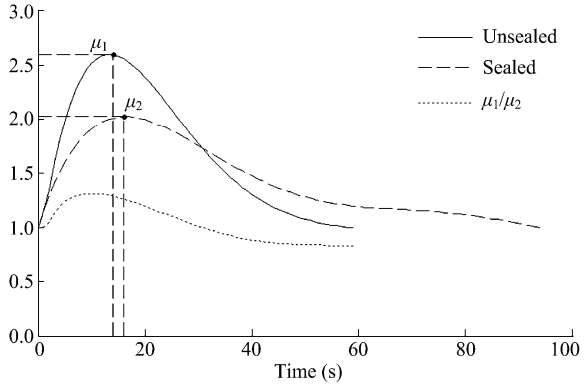

Fig. 6 Deformation rate of the sealed and unsealed soft rays.

Table 1 Performance comparison between the two soft rays

Performances	Sealed	Unsealed
Adaptive environment	Underwater, land	Land
Large deformation capability	Weak	Strong
Response speed	Slow	Fast
Supporting body force	Small (underwater)	Large (land)

By considering other factors (*e.g*., environmental conditions, comprehensive characteristics, *etc*.) and by comparing the performance of the two soft ray designs (Table 1), the sealed soft ray is seen to be suitable in underwater environments, whereas the unsealed ray is suitable for terrestrial environments. As we focus on a soft bionic platform in a terrestrial environment in this study, the unsealed soft ray design was considered.

3.3 Key parameters

Cole[19] found a correlation between the length of a ray and the frequency, with which it moves in advance, by investigating a series of 116 specimens, that was, the uniformity of the ray length can help to achieve efficient locomotion[18,19]. Table 2 shows the main parameters of the soft robot prototype. The bionic robot based on silicone rubber could be light, and its size was nearly identical to that of a biological sea star.

Table 2 Key parameters and values of the soft robot prototype

Parameters	Value
Mass	145 g
Number of the soft robot ray	5
Number of SMA spring	5
Coil diameter of SMA spring (d)	0.52 mm
SMA spring external diameter (D)	3.64 mm
Looping number of SMA spring	24
Mean width of the soft robot ray	26.1 mm
Mean thickness of the soft robot ray	12.2 mm
Working length of the SMA spring	73.9 mm
Length of the soft robot ray	93.2 mm
Radius of the soft robot	114.0 mm

3.4 Modeling the SMA actuators

The water-vascular system of a sea star is a hydraulic system that consists of a network of fluid-filled canals. The system is also concerned with locomotion[17]. Adopting an artificial hydraulic system for a soft robot remains a considerable challenge. However, SMA actuators have an extremely large energy density per cycle and a power to weight ratio[25–27]. By considering the large-scale and relatively small driving force characteristics of elastic deformation, we chose SMA springs as the actuators for the starfish-like soft robot.

Martensitic (reverse) transformation is an important base for SMA deformation[25,28,29]. In this study, we selected reverse martensitic transformation to reveal the mechanism of the driving deformation of a heated SMA spring. Fig. 7 displays the three basic stages in reverse transformation, namely, detwinned martensite, martensite–austenite, and austenite, the corresponding contracting states of the spring, and the relationship among heating temperature T, austenitic starting temperature A_S, and ending temperature A_F. In this study, P is the elastic restoring force of the SMA spring, and its value increases to maximum as reverse martensitic transformation proceeds. Contraction of the heated spring causes continuous bending deformation of the soft body during the total reverse transformation, and the spring can return to its initial state when cooling.

To analyze the thermo-mechanical property of the SMA spring under martensitic (reverse) transformation, we developed a deformation model of the SMA spring wire with a bias spring load, as shown in Fig. 8a. The external load P is

$$P=K\delta, \tag{2}$$

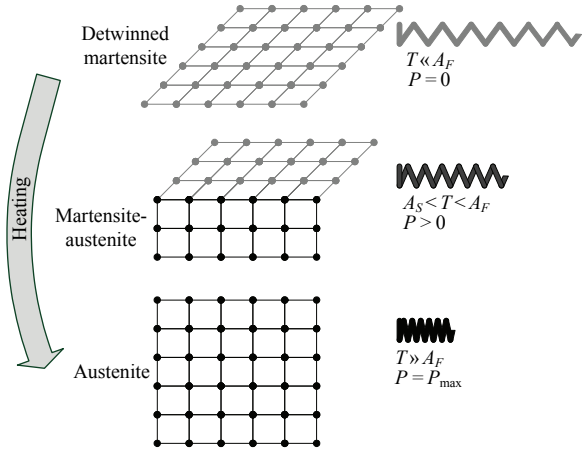

Fig. 7 The three basic states of a Ni-Ti SMA spring actuator during the reverse martensite phase transformation and the corresponding deformation states, dot-position relationship, temperature, and force analysis of the spring.

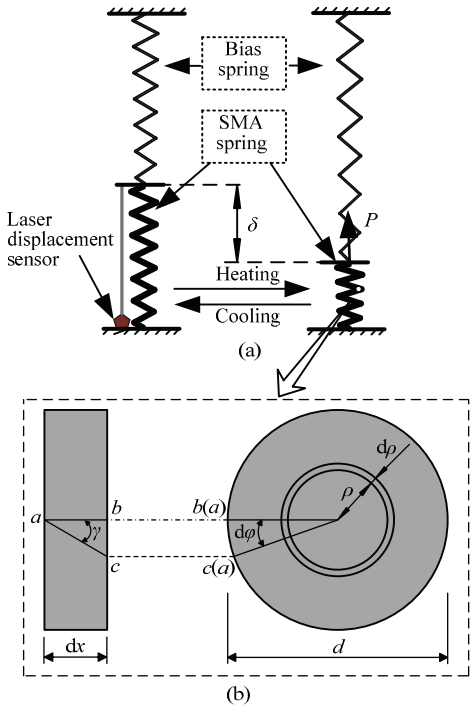

Fig. 8 Displacement analysis of an SMA spring actuator with a bias spring load. (a) Actuation of the SMA spring actuator with a bias spring load; (b) cross section of the SMA spring wire.

where K is bias spring stiffness coefficient and δ is the elastic displacement.

Fig. 8b shows the mechanical characteristics and thermo-elasticity of the deformation and return of the SMA spring under martensitic (reverse) transformation from a micro perspective via force analysis of a cross section of a heated spring wire. It is assumed that a uniform torque only occurs on the cross section; thus, a linear variation of shear stress is presented along the

radius direction. The shear stress is $2\rho\tau/d$ at distance ρ from the center, where d is the diameter of the SMA spring wire. After establishing the integral for ρ via the torque attracted by the annular width dρ, if the overall torque is PR when the heated spring is in a fully retracted state, the shear stress is then given by

$$\tau = k\frac{16PR}{\pi d^3}, \tag{3}$$

where k is the stress correction factor, P is the load, and R is the radius of the spring. By setting the spring index C ($C=D/d$), where D is the diameter of the spring, the stress correction factor can be obtained by using the Wahl formula[29] as

$$k = \frac{4C-1}{4C-4} + \frac{0.615}{C}. \tag{4}$$

The shear strain can be calculated by using Eq. (3) as

$$\gamma = \frac{\tau}{G} = k\frac{16PR}{\pi d^3 G}, \tag{5}$$

where G is the shear modulus.

As shown in Fig. 8b, the trace rotary will be dφ = 2γdx/d because line ab, which is parallel to the axis, distorts angle γ to line ac. When the spring length is πnD in the fully retracted state, the twist angle from Eq. (5) is given by

$$\varphi = \int_0^{\pi nD} \mathrm{d}\varphi = \int_0^{\pi nD} \frac{2\gamma}{d}\mathrm{d}x = k\frac{64PR^2 n}{Gd^4}. \tag{6}$$

The displacement is then

$$\delta = R\varphi = k\frac{8PD^3 n}{Gd^4}. \tag{7}$$

According to the preceding deformation analysis of the SMA spring actuator, an experiment was conducted on the heated SMA spring to find out the deformation under different loads by varying bias spring stiffness, including 320 N·mm, 160 N·mm, 80 N·mm, 0 N·mm, respectively. The original length of SMA spring wire is 15 mm, and at working state it is 70 mm without load. The SMA spring wire deformation displacement was measured by laser displacement sensor. The wire diameter and the external diameter of the SMA spring were 0.52 mm and 3.64 mm, respectively. The current exerting on the SMA spring wire was 2 A and the heating time was 20 s.

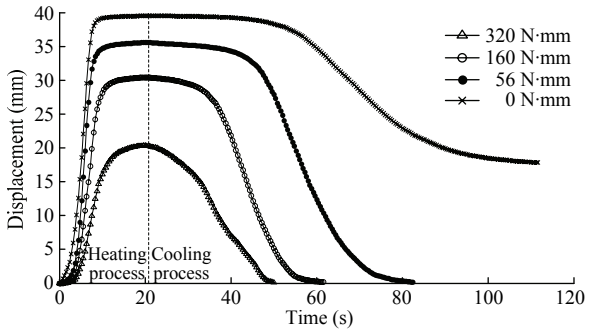

Fig. 9 Displacements of the SMA spring wire under different stiffness bias spring loads.

As shown in Fig. 9, the deformation displacement of SMA spring wire reduces as the bias spring stiffness increases. On the other hand, the external load obviously affects the cooling process as the cooling time is shorter when stiffness increases. The SMA spring wire back to its previous position with an external load and the crystal is detwinned martensite at this time. However, when the bias spring stiffness is zero, which implies that no external load, the SMA spring wire cannot recover because the crystal transform from austenite into self-accommodation martensite.

The deformation analysis of the SMA spring actuator is considered as a useful reference for the deformation control and experiments in various terrains. With this model, the SMA spring, which functions as the artificial actuator, can be easily designed and controlled according to the displacement and force requirements of the experiments.

4 Locomotion and control strategy

Multi-gaits and a suitable control strategy are key factors to improve the environmental adaptability of soft robots[4,30,31]. One SMA spring actuator is embedded into each soft ray. Hence, the contraction or relaxation in length of each actuator causes the respective ray to bend and establish the motion of the robot. The robot moves in a specific trajectory and steered track with the control strategy. Given that the shape memory actuation is a thermal process, the efficiency of these actuators can be improved by rapid pulses of high currents than by slow pulses of low currents. An open-loop sequential control was applied to the SMA spring coils.

4.1 Moving strategy on flat ground

Fig. 10 presents the schematic of the control planner and the multi-gait pattern for multi-gait that follows the

locomotion strategy (Figs. 1 and 2). As shown in Fig. 10a, the controller synthesizes information from the behavior decision module, as well as the basic behavior and environment information module, and then sends the control signal to the SMA actuators of the robot in different environmental conditions. Control strategy and path planning for soft robots involve deforming soft appendages to adjust to the environment or to navigate through confined spaces. Based on the locomotion strategy described in the previous section, Fig. 10b shows the gait planning strategy of the robot prototype for crawling on sand, creeping on a clammy rough terrain, and moving on transitional media (which is called pattern *AB–CD–E* and involves five main steps). The SMA spring coils *A* and *B* were activated in the first time step, *C* and *D* in the second time step, and *E* in the third time step. In the last two time steps, all spring coils were cooling.

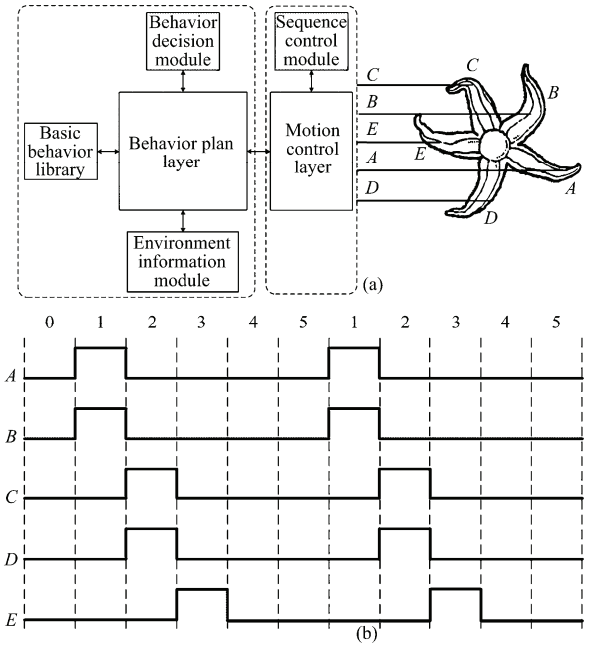

Fig. 10 Control strategy. (a) Schematic of the control system; (b) multi-gait patterns applied to SMA actuators for crawling on sand and creeping on a clammy rough terrain.

4.2 Strategy for passing through obstacle

For a bionic robot, the ability to negotiate through a rocky terrain and to avoid an impassable obstacle is related to its ability to adapt to a new or complex environment. By negotiating through an obstacle and by applying gait transition to avoid an obstacle (Figs. 3a and 3b), the corresponding strategies of the multi-gait pattern that can carry out straight and turning gaits was developed, as described in Fig. 11.

4.3 Rolling strategy

Starfish typically move forward to the coast along with tidewater when the tide rises, whereas other starfish return to the ocean by following the tidewater during its fall; others may remain on the coastal beach or on rugged rocks[14,16,32]. A sea star that is leaving a rugged surface rock may move ahead by manipulating its tiny feet slowly or by using its water-vascular system to curl up its entire body and then to roll on the rock rapidly[18,24,29]. Inspired by this natural phenomenon, we designed an experiment to examine whether the robot prototype can roll from a rough rock to sand or clammy rough terrain. The gait multi-gait pattern *ABCDE* was applied and all the rays of the robot were activated to generate a large deformation.

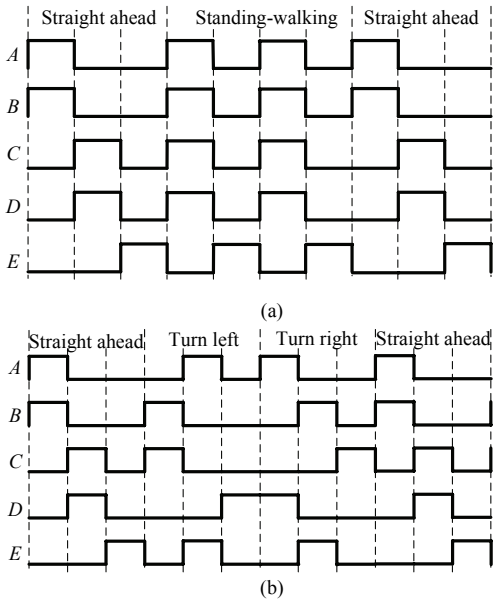

Fig. 11 Multi-gait patterns (a) for navigating through a small obstacle and (b) in avoiding an obstacle.

5 Experimental setup and results

To demonstrate how a sea star can achieve different gaits and move with two rays in advance in various terrains, we studied the multi-gait locomotion of the soft robot prototype in different terrain conditions, as listed in Table 3, via experimental observation. Moving gaits, including crawling, were selected based on the peripheral environments wherein the robot is exploring. The results reveal the effectiveness of the proposed locomotion strategy and the control strategy as discussed in section **4**. Considering that the cycle frequencies of the SMA spring actuators are limited by passive cooling

during the restoration phase, which are sensitive to environmental conditions, such as air flow and ambient temperature, all experiments were conducted in an indoor place where the temperature maintained around 20 ˚C. Fig. 12 displays an overview of the soft robot prototype made by using the 3D printing model.

5.1 Crawling on sand

Sand is a common intertidal zone habitat of echinoderms, including starfish, when they are washed ashore[19,33]. Similar to an actual sea star, the five-ray soft robot prototype can crawl smoothly on dry sand (Fig. 13), and leave obvious traces via a zigzag movement. The locomotion strategy and multi-gait pattern *AB–CD–E* were applied to the SMA actuators.

5.2 Creeping across a clammy rough terrain

A sea star frequently lingers in the intertidal zone, including on clammy rough grounds[18]. Fig. 14 displays a sequence of snapshots of this prototype. Multi-gait pattern *AB–CD–E* was applied to the SMA actuators. As shown in Fig. 14, the starfish-like soft robot moves with a creeping or analogous peristaltic motion on a clammy rough terrain. During one complete movement period, in accordance with the locomotion strategy (Fig. 2) and the multi-gait pattern (Fig. 10b), soft rays *A* and *B* bent largely at $T_1 = 8$ s (Fig. 14b), rays *C* and *D* bent at $T_2 = 17$ s (Fig. 14c), and ray *E* bent at $T_3 = 31$ s (Fig. 14d). Rays *A* and *B* relaxed fully at $T_4 = 42$ s (Fig. 14e), and rays *C* and *D* relaxed at $T_5 = 53$ s (Fig. 14f). The arrows in Figs. 14a and 14f show the initial position of the soft robot.

5.3 Navigating through an obstacle

Most starfish, particularly those inhabiting a coastal area with many cobble stones[17,21], typically negotiate over small obstacles via coordinating actuation of five rays. Based on the proposed locomotion strategy and the multi-gait pattern (Figs. 3a and 11a), the robot prototype has successfully negotiated an obstacle that is 23.2 mm in height (approximately twice its body height of 12.2 mm) in the rocky terrain, as shown in Fig. 15. The results illustrate that the gait mode and the control strategy are effective, enabling the soft robot to navigate across an obstacle.

5.4 Bypassing an obstacle

When the starfish-like robot encounters an im-

Table 3 Experimental exploration arrangements

Environmental condition	Gait mode	Control pattern
Sand	Crawling	*AB–CD–E*
Clammy floor	Creeping	*AB–CD–E*
Small obstacle	Navigating	*AB–CD–E/ ABCD–E/ AB–CD–E*
Impassable obstacle	Bypassing	*AB–CD–E/ BC–AE–D/ AD–BE–C/ AB–CD–E*
Rock	Rolling	*ABCDE*

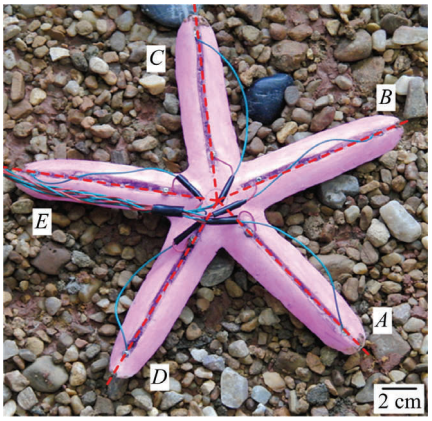

Fig. 12 The soft robot showing the notations of the rays. Dotted lines denote the axis of radial symmetry with respect to the prototype.

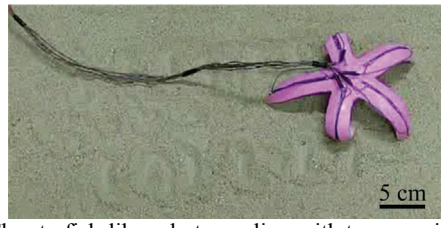

Fig. 13 The starfish-like robot crawling with two rays in advance on dry sand.

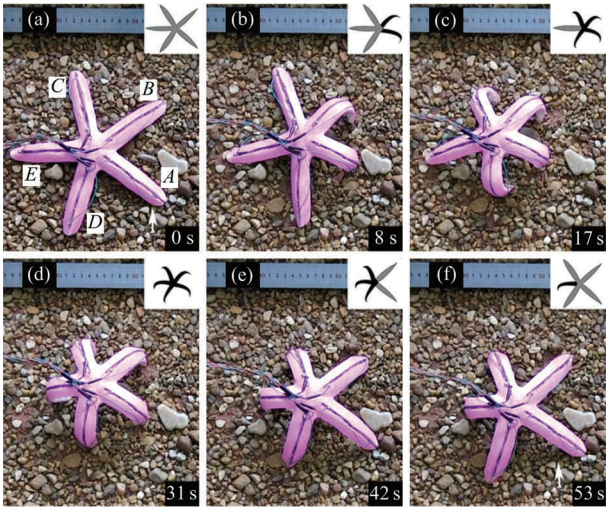

Fig. 14 (a–f) Complete cycle of the creeping gait that takes 53 s; the particular ray(s) actuated in each step are shown (in insets) as deep black, whereas the inactive ray(s) are shown (in insets) as light gray. (Insets are small. Difference of stages is not obvious).

passable obstacle (approximately several times its size), the robot can steer clear of the obstacle by changing its gait mode and multi-gait pattern. Fig. 3b shows that the soft robot succeeded in bypassing a rock by employing the locomotion strategy of gait transition and multi-gait pattern (Fig. 11b), as shown in Fig. 16. The experimental results indicate that the robot can turn by regulating the timing sequence of the multi-gait pattern for the rays and for gait motions. The control pattern was changed from *AB–CD–E* to *BC–AE–D*, and then to *AD–BE–C*.

5.5 Rolling motion on rough rocks

A sea star is frequently found on rocky shores during falling tide, and its locomotion in such an environmental condition depends on the rays that are curled upward to their tips[18,34]. Nevertheless, we found an effective motion for the robot to leave the rocks. By using the rolling locomotion pattern, the prototype has succeeded in completing the rolling motion, as displayed in Fig. 17.

6 Results

We have discussed the locomotion strategy, multi-gait patterns, and experimental investigation for the soft robot prototype. The results demonstrate the multi-gait and robustness of the prototype in various terrains. In this section, we compare the results of the prototype crawling in two different circumstances (*i.e.*, sand and clammy rough grounds) and then discuss the interaction between mobility and environmental terrain.

The distance traveled of the starfish-like soft robot during a full moving cycle can be expressed by

$$s = \sum_{i=1}^{3} l_{si} + \sum_{i=4}^{6} l_{ri} - \varepsilon, \tag{8}$$

where l_{si} is the distance of the forward movement of the soft robot when a group of rays *AB*, *CD*, and *E* contracted, i = 1, 2, 3; l_{ri} is the distance of the forward movement of the soft robot when a group of rays *AB*, *CD*, and *E* relaxed, i = 4, 5, 6; ε is the backward slippage distance of the soft robot during its forward motion caused by instantaneous excessive friction or instability.

The displacement information of the prototype crawling on sand has been extracted by the recording video (by OpenCV). Fig. 18 display the steps to process the video, including obtaining data structure and images, binarization, extracting the motion model and limit po-

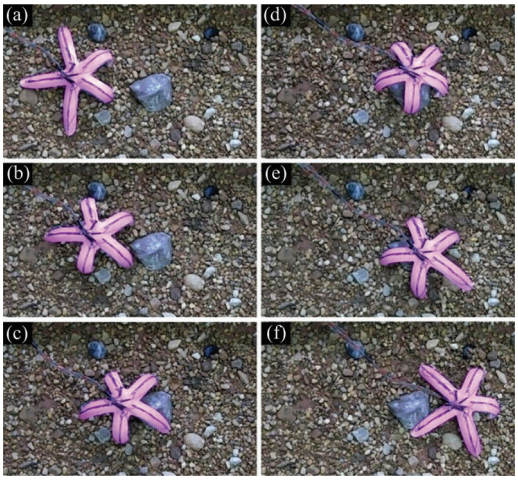

Fig. 15 The soft robot walking through a rocky terrain.

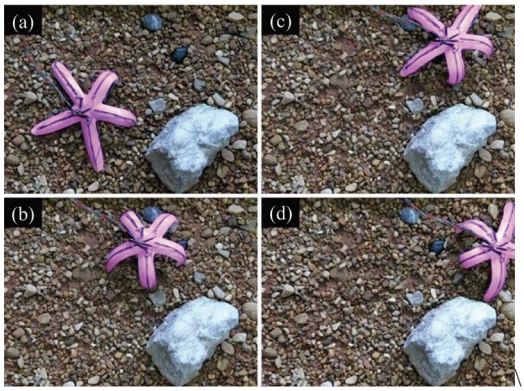

Fig. 16 The soft robot bypassing around an obstacle.

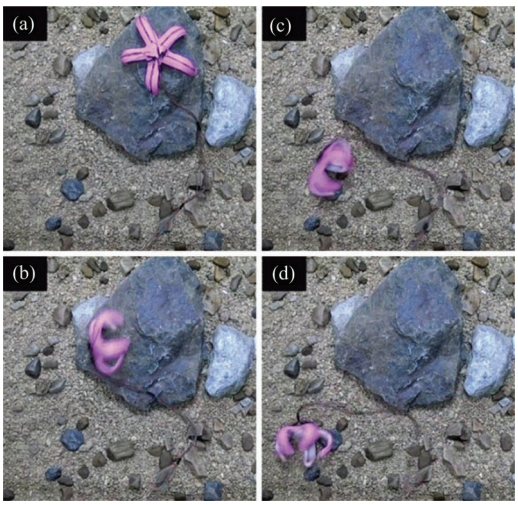

Fig. 17 The rolling motion of the soft robot on rough rock.

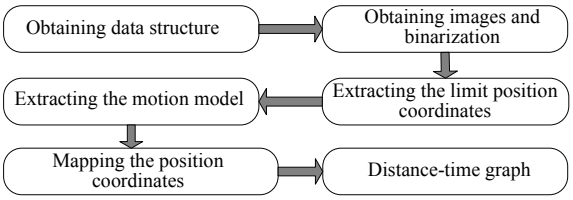

Fig. 18 Steps to acquire the crawling displacement.

sition coordinates of the prototype, and coordinate mapping. The displacement–time graph of the soft robot is shown in Fig. 19a. The average value of moving step was 50.7 mm during one moving cycle, and the prototype crawled 456 mm at an average speed of 130 mm·min^{-1}. The motion characteristic of the soft robot is comparable to that of the biological starfish. The crawling gait on sand exhibits an approximate periodicity (approximately eight motion cycles in this experiment).

The displacement–time graph for the robot creeping on a clammy rough terrain is shown in Fig. 19b. The soft robot crept 248 mm within an average speed value of 20.7 mm·min^{-1}, and the average value of moving step was 35.4 mm during one moving cycle. Fig. 19b displays the zigzag locomotion path of the soft robot and a soft animal on rough conditions. Fig. 20 depicts the comparison on the movement in different terrains, including the average value of moving step and speed.

The results indicate that the flexible motion characteristic of the soft robot prototype is similar to the locomotion of soft-bodied organisms in different environmental media (*e.g*., sand and clammy rough terrain). The speed of the prototype crawling on the sand was nearly 6.5 times the speed on a clammy rough terrain, because of the different mechanical properties between the robot prototype and the medium surface. The environmental condition also affects the frequencies of the SMA spring actuators, and is thus an important factor to improve the speed of the robot in various gaits.

7 Conclusion and future work

The present work primarily aims to demonstrate how a soft robot inspired by starfish can achieve deformability, mobility, rough terrain locomotion, and multi-gaits by using SMA actuators. Several research issues in soft robots have been identified. A bionic design, basic locomotion strategy, control strategy, and experiments have been presented for a starfish-like soft robot to address such issues. We constructed different soft rays and conducted deformation analysis. A model of SMA actuators was developed. Through this model, the SMA spring can be precisely designed and controlled according to the displacement and force requirements. Multi-gait locomotion (*i.e.*, crawling, creeping, navigating, bypassing, and rolling) can be achieved by applying appropriate control patterns and the related locomotion strategy of the soft robot.

The work presented also contributes to soft robotics. The prototype demonstrates its mobility adaptive to different terrains and tasks. Using only five soft rays actuated by SMA actuators, the robot is able to achieve a large deformation and crawl on dry sand and creeps on a clammy rough terrain by following the gait pattern *AB–CD–E*. The robot also successfully navigates through an obstacle that is 23.2 mm high and over rocky terrain via patterns *AB–CD–E* and *ABCD–E*. Through the gait transition with strategy changes in patterns *AB–CD–E*, *BC–AE–D*, and *AD–BE–C*, the robot is able

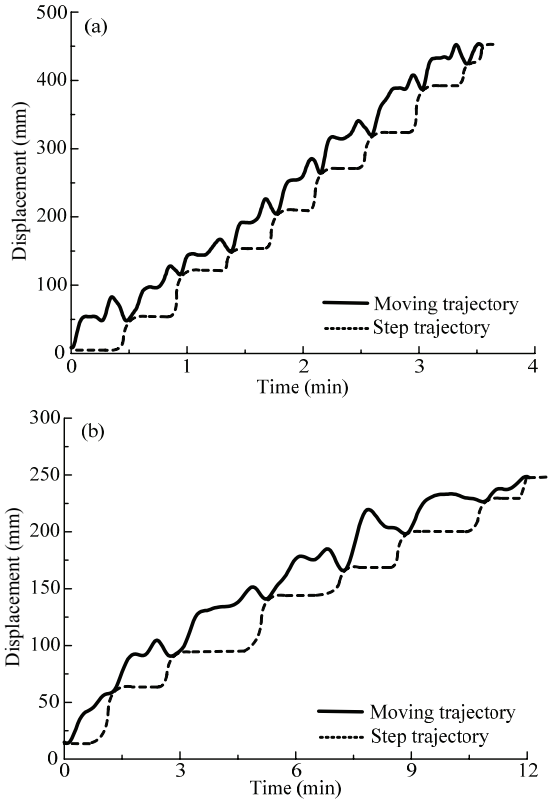

Fig. 19 Displacement of the prototype. (a) Crawling on sand; (b) creeping on a clammy rough terrain.

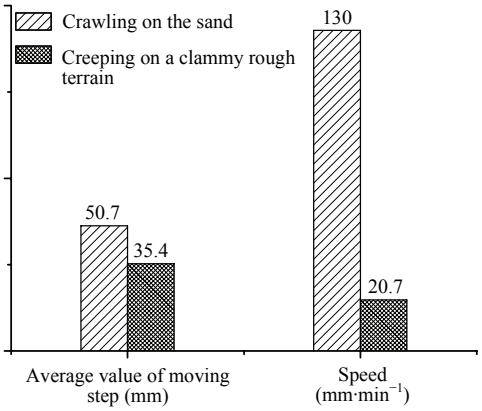

Fig. 20 The contrastive analysis on the performance in different terrains, including the average value of moving step and speed.

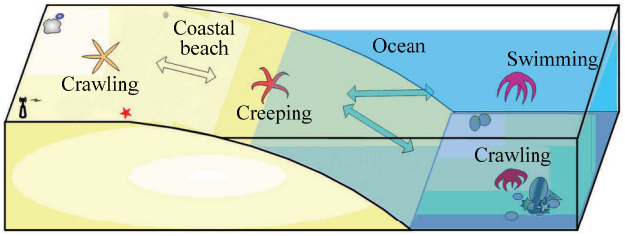

Fig. 21 An amphibious soft robot with multiple motions and high adaptability in various environments.

to avoid a large obstacle in front of it. By using only the control pattern *ABCDE*, the soft robot rolls on rough rocks and continues to crawl ahead.

The experiments presented several limitations of the current prototype, such as underwater velocity, autonomy, and adaptability. In future works, we aim to develop a soft robot with multiple motions and high adaptability in both terrestrial and aquatic environments, as shown in Fig. 21. The improved soft robots are expected to possess an optimal structure with flexible capabilities, a continual planner, wireless communication, *etc*.[35,36]. Several challenges remain, such as the optimized design and fabrication of the soft robot and the methodology for modeling a soft body, robustness in uncertain or changing environments, *etc*. On the other hand, an accurate locomotion analysis requires the modeling of flexible rays by considering the nonlinear and large deformation.

Acknowledgment

The authors would like to acknowledge the support of the National Natural Science Foundation of China (Grants. 51105349, 61375095, 51275501). We are grateful to Fei Li and Chunshan Liu for their assistance in the experiments.

References

[1] Lee D V, Biewener A A. Big dog-inspired studies in the locomotion of goats and dogs. *Integrative and Comparative Biology*, 2011, **51**, 190–202.

[2] Trivedi D, Rahn C D, Kier W M, Walker I D. Soft robotics: Biological inspiration, state of the art, and future research. *Applied Bionics and Biomechanics*, 2008, **5**, 99–117.

[3] Altendorfer R, Koditschek D E, Holmes P. Stability analysis of a clock-driven rigid-body SLIP model for RHex. *International Journal of Robotics Research*, 2004, **23**, 1001–1012.

[4] Yamada H, Takaoka S, Hirose S. A snake-like robot for real-world inspection applications: The design and control of a practical active cord mechanism. *Advanced Robotics*, 2013, **27**, 47–60.

[5] Shepherd R F, Ilievski F, Choi W, Morin SA, Stokes A A, Mazzeo A D, Chen X, Wang M, Whitesides G M. Multigait soft robot. *Proceedings of the National Academy of Sciences*, 2011, **108**, 20400–20403.

[6] Correll N, Önal Ç D, Liang H, Schoenfeld E, Rus D. Soft autonomous materials–using active elasticity and embedded distributed computation. In: Khatib O, Kumar V, Pappas G (eds). *Experimental Robotics*, the 12*th International Symposium on Experimental Robotics*, Essaouira, Morocco, 2014, 227–240.

[7] McMahan W, Chitrakaran V, Csencsits M, Dawson D, Walker I D, Jones B A, Pritts M, Dienno D, Grissom M, Rahn C D. Field trials and testing of the OctArm continuum manipulator. *Proceedings of the IEEE International Conference on Robotics and Automation*, Orlando, USA, 2006, 2336–2341.

[8] Calisti M, Arienti A, Giannaccini M E, Follador M, Giorelli M, Cianchetti M, Mazzolai B, Laschi C, Dario P. Study and fabrication of bioinspired octopus arm mockups tested on a multipurpose platform. *IEEE RAS and EMBS International Conference on Biomedical Robotics and Biomechatronics*, Tokyo, Japan, 2010, 461–466.

[9] Bar-Cohen Y. Actuation of biologically inspired intelligent robotics using artificial muscles. *Industrial Robot*, 2003, **30**, 331–337.

[10] Otake M, Kagami Y, Kuniyoshi Y, Inaba M, Inoue H. Inverse dynamics of gel robots made of electro-active polymer gel. *Proceedings of the IEEE International Conference on Robotics and Automation*, Taipei, 2003, 2299–2304.

[11] Seok S, Onal C D, Wood R, Rus D, Kim S. Peristaltic locomotion with antagonistic actuators in soft robotics. *Proceedings of the IEEE International Conference on Robotics and Automation*, Anchorage, Alaska, USA, 2010, 1228–1233.

[12] Shiotsu A, Yamanaka M, Matsuyama Y, Nakanishi H, Hara Y, Tsuboi T, Iwade T, Sugiyama Y, Hirai S. Crawling and jumping soft robot KOHARO. *Proceedings of the* 32*nd International Symposium on Robotics*, Seoul, Korea, 2005, 134–140.

[13] Lin H T, Leisk G G, Trimmer B. GoQBot: A caterpillar-inspired soft-bodied rolling robot. *Bioinspiration & Biomimetics*, 2011, **6**, 026007.

[14] Anna K. Antarctic starfish, Odontastervalidus, distinguish between fed and starved conspecifics. *Polar Biology*, 2001, **24**, 408–410.

[15] Haesaerts, Delphine, Jangoux M, Flammang P. Adaptations to benthic development: Functional morphology of the at-

tachment complex of the brachiolaria larva in the sea star *Asterina gibbosa*. *Biological Bulletin*, 2011, **211**, 172–182.

[16] Ormond R F G, Hanscomb N J, Beach D H. Food selection and learning in the crown‐of‐thorns starfish, *Acanthaster planci* (L). *Marine Behaviour and Physiology*, 1976, **2**, 93–105.

[17] Lawrence J M. *Starfish*: *Biology and Ecology of the Asteroidea*, JHU Press, Baltimore, USA, 2013.

[18] Starfish, [2014-04-11], http://en.wikipedia.org/wiki/starfish

[19] Cole L J. Direction of locomotion of the starfish (Asterias-forbesi). *Journal of Experimental Zoology*, 1913, **14**, 1–32.

[20] Chia F S. Some observations on the development and cyclic changes of the oöcytes in a brooding starfish, *Leptasterias-hexactis*. *Journal of Zoology*, 1968, **154**, 453–461.

[21] Sahai R. The starfish twins: two young planetary nebulae with extreme multipolar morphology. *Astrophysical Journal Letters*, 2000, **537**, L43.

[22] Gurarie E, Andrews R D, Laidre K L. A novel method for identifying behavioural changes in animal movement data. *Ecology Letters*, 2009, **5**, 395–408.

[23] Harvey C, Garneau F X, Himmelman J H. Chemodetection of the predatory seastar *Leptasterias polaris* by the whelk *Buccinum undatum*. *Marine Ecology Progress Series*, 1987, **40**, 79–86.

[24] Pincebourde S, Sanford E, Helmuth B. An intertidal sea star adjusts thermal inertia to avoid extreme body temperatures. *American Naturalist*, 2009, **174**, 890–897.

[25] Eggeler G, Hornbogen E, Yawny A, Heckmann A, Wagner M. Structural and functional fatigue of NiTi shape memory alloys. *Materials Science and Engineering*, 2004, **378**, 24–33.

[26] Wang Z, Li J, Hang G, Wang Y. A flexible hingeless control surface inspired by aquatic animals. *Journal of Bionic Engineering*, 2010, **7**, 364–374.

[27] Zakerzadeh M R, Sayyaadi H. Experimental comparison of some phenomenological hysteresis models in characterizing hysteresis behavior of shape memory alloy actuators. *Journal of Intelligent Material Systems and Structures*, 2012, **23**, 1287–1309.

[28] Muhammad A, Nguyen Q V, Park H C, Hwang D Y, Byun D, Goo N S. Improvement of artificial foldable wing models by mimicking the unfolding/folding mechanism of a beetle hind wing. *Journal of Bionic Engineering*, 2010, **7**, 134–141.

[29] Otsuka K, Wayman C M. *Shape Memory Materials*. Cambridge University Press, Cambridge, 1999.

[30] Crespi A, Ijspeert A J. Online optimization of swimming and crawling in an amphibious snake robot. *IEEE Transactions on Robotics*, 2008, **24**, 75–87.

[31] Aoi S, Kazuo T. Locomotion control of a biped robot using nonlinear oscillators. *Autonomous Robots*, 2005, **19**, 219–232.

[32] Takeda S, Yasushi K. Preliminary study of management of red tide water by the filter feeder *Mytilus edulis* gallo-provincialis. *Marine Pollution Bulletin*, 1994, **28**, 662–667.

[33] Hendler G, Franz D R. The biology of a brooding sea star, *Leptasterias tenera*, in Block Island Sound. *Biological Bulletin*, 1982, **162**, 273–289.

[34] O'Neill P. Structure and mechanics of starfish body wall. *Journal of Experimental Biology*, 1989, **147**, 53–89.

[35] Flocchini P, Prencipe G, Santoro N, Widmayer P. Arbitrary pattern formation by asynchronous, anonymous, oblivious robots. *Theoretical Computer Science*, 2008, **407**, 412–447.

[36] O'Grady R, Groß R, Christensen A L, Dorigo M. Self-assembly strategies in a group of autonomous mobile robots. *Autonomous Robots*, 2010, **28**, 439–455.